



HAL
open science

How chemical defects influence the charging of nanoporous carbon supercapacitors

Romain Dupuis, Pierre-Louis Valdenaire, Roland J.-M. Pellenq, Katerina Ioannidou

► **To cite this version:**

Romain Dupuis, Pierre-Louis Valdenaire, Roland J.-M. Pellenq, Katerina Ioannidou. How chemical defects influence the charging of nanoporous carbon supercapacitors. Proceedings of the National Academy of Sciences of the United States of America, 2022, 119 (17), 10.1073/pnas.2121945119 . hal-03920236v1

HAL Id: hal-03920236

<https://hal.science/hal-03920236v1>

Submitted on 31 May 2022 (v1), last revised 5 Feb 2024 (v2)

HAL is a multi-disciplinary open access archive for the deposit and dissemination of scientific research documents, whether they are published or not. The documents may come from teaching and research institutions in France or abroad, or from public or private research centers.

L'archive ouverte pluridisciplinaire **HAL**, est destinée au dépôt et à la diffusion de documents scientifiques de niveau recherche, publiés ou non, émanant des établissements d'enseignement et de recherche français ou étrangers, des laboratoires publics ou privés.

How chemical defects influence the charging of nanoporous carbon supercapacitors

Romain Dupuis^{a,b,c}, Pierre-Louis Valdenaire (the late)^c, Roland J.-M. Pellenq^{c,d}, and Katerina Ioannidou^{b,c}

^aIEM and ICGM, Univ. Montpellier, CNRS, Montpellier, France; ^bLMGC, Univ. Montpellier, CNRS, Montpellier, France; ^cMIT/CNRS/Aix-Marseille Université Joint Laboratory "MultiScale Materials Science for Energy and Environment", UMI MSE2, Massachusetts Institute of Technology, 77 Massachusetts Avenue, Cambridge, Massachusetts 02139, USA; ^dInternational Research Laboratory, EPIDAPO, CNRS-George Washington U., Washington DC

This manuscript was compiled on May 30, 2022

Ion desolvation and confinement are key physical processes in porous-carbon based supercapacitors undergoing charging and discharging cycles. We investigate electrolyte interactions between polarized porous carbon with subnanometer pore sizes and aqueous sodium chloride electrolyte using molecular dynamics. Inspired by recent first principles calculations, we developed a scheme accounting for chemical defects in electrodes where only the non-sp² carbons species carry an extra negative charge (on the anode) and an extra positive charge (on the cathode) due to voltage polarization. This drives electrolyte species (ions and solvent molecules ; water in this work) to adsorb at the electrode surface and in subnanometric pores upon polarization. First we observe an asymmetrical desolvation process of sodium and chloride ions at the external surface of the electrodes. The ionic distribution at the external surface of the electrodes is consistent with the Debye-Hückel electric potential equation and empirical trends observed for non-porous electrodes. In a second stage, we demonstrate that the nanoporosity of the electrodes is filled with ions and scarce water molecules and contributes to about 20% of the overall capacitance. A fraction of desolvated ions are irreversibly trapped in the core of electrodes during discharge. While maintaining the overall electroneutrality of the simulation cell, we found that anodes and cathodes do not carry the same amount of ions at all time steps leading to charge imbalance.

Ionic adsorption | Molecular dynamics | dehydration

Understanding ions in nano-confinement is the key element to get the fundamental physical basis of electrochemical energy storage underlying modern electrochemistry devices like batteries and supercapacitors (1, 2). In particular, fundamental understanding of the ionic adsorption processes and confinement inside nanoporous carbon electrodes is essential for predicting and improving the capacitance (3) or deionisation efficiency of carbon-based devices (4, 5). Recent in situ X-ray (6) and neutron scattering (7) have shown that subnanometric pores of carbon electrodes enhance the ionic adsorption and its overall capacitance performance (8). In fact, if the pores are of the same size as electrolyte ions, high capacitances (leading to the term supercapacitor) have been observed that does not follow existing theories and empirical trends (9–12).

The term of electrical double layer (EDL) capacitor comes from the classical picture of non porous electrodes that accumulate oppositely charged ions at their vicinity upon voltage polarisation in a mean-field dielectric continuum description of the solvent populated with point charged ions at a given concentration. This picture although very popular obviously does not hold for porous electrodes with sub nanometric pores. In particular, the mean-field Gouy–Chapman–Stern description of a EDL fails in high molar concentrations and for pore

sizes smaller than a few nanometers (typically 4 nm for carbon substrates) (13, 14). EDL predictions usually rely on the Poisson-Boltzmann theory and modified versions such as Debye-Hückel (15, 16) and Donnan models (17). More recent approaches based on thermodynamics theory for heterogeneous ionic fluids allow to take into account ionic size hence ionic position correlations(18). Recently, this statistical physics description of an EDL theoretical prediction was extended to include time dependence and study the dynamics of the ionic charging process of a planar electrode (19).

Presently, there is no theory capable of solving the electrostatics problem for ions confined in the nanopores of a disordered porous carbon material commonly used in electrochemical devices. Nowadays, atomistic simulation techniques implement statistical physics methods that are able of describing both the intrinsic textural disorder of a porous carbon materials at the nanoscale and the movement of electrolyte species (solvent molecules and ions) in their pores under operational functioning conditions of a supercapacitor device (i.e. under polarization) (20–23).

There are currently two main approaches to describe atomic systems under polarization, the constant voltage (CV) and the constant charge (CC) methods. (i) The CV approach assumes a perfectly conducting substrate hence accumulating/depleting charges only on the atoms at the pore and external surfaces with no regards to the intrinsically defective nature of porous

Significance Statement

Nanoporous carbon texture makes fundamental understanding of the electrochemical processes challenging. Based on DFT results, the proposed atomistic approach takes into account topological and chemical defects of the electrodes and attributing them a partial charge that depends on the applied voltage. Using a realistic carbon nanotexture, a model is developed to simulate the ionic charge both at the surface and in the subnanometric pores of the electrodes of a supercapacitor. Before entering the smallest pores, ions dehydrate at the external surface of the electrodes leading to an asymmetric adsorption behavior. Ions in subnanometric pores are mostly fully dehydrated. The simulated capacitance is in qualitative agreement with experiments. Part of these ions remain irreversibly trapped upon discharge.

R.D, K.I, and R.P. designed, wrote the manuscript, discussed and analyzed the results, R.D. and P.-L. V. performed the calculations

Authors declare no competing interests.

²To whom correspondence should be addressed. E-mail: aikaterini.ioannidou@umontpellier.fr, romain.dupuis@umontpellier.fr

carbons (see Fig. 1(a)). Applied to porous carbon materials, the CV approach thus assumes that all carbon atoms are in the sp² hybridisation state, i.e. conducting electrons. The main assumption of the CV method is, therefore, the metallic approximation - the electrodes are considered ideal conductors with no localisation of electric charge except at the material boundaries in contact with the electrolyte. In recent simulation works(10), pore surfaces are treated as an extension of the external electrode surface. It is important to indicate that the charging process of substrate atoms is in the order of fs while ion diffusion occurs at the scale of ns (24, 25). Thus upon polarisation, the charges on the solid matrix species attract ions first. Once equilibrium is reached, thermal agitation of adsorbed ions can induce (in a constant voltage description) charge fluctuation on electrode atoms that in turn can redistribute ions in their vicinity. This is the main advantage of the CV approach; its main drawback is that it ignores charge localisation due to chemical heterogeneity. As a result, within the CV approach, ion docking is only observed at the external surfaces of the electrodes or in large nanopores; the subnanopores being found not to participate to the capacitance in sharp contrast to experiment of activated carbon based super-capacitors (see Fig. 1(b))(3).

(ii) The standard CC approach gives all substrate atoms the same fixed charge. The main drawback of the CC approach is that substrate charges are not allowed to fluctuate upon ion docking. Thus, this method only simulates the initial ion docking dynamics before charge self-regulation takes place. In the literature, it was reported that the CC approach may lead to an unphysical temperature increase(26). In the supplementary materials we give evidence that this issue might come from the configurational setup of the simulation cell with bouncing walls for ions in a rigid electrodes approximation. With a full periodic cell simulating a stack of immersed electrodes, using NVE simulation under polarization we found that the temperature was well tempered (after initial relaxation at 300K). However, this leads to unphysical ion docking deep in the electrodes regardless the pore size (see Fig. 1(b)). In sum, both the standard CC and CV methods fail for different reasons hence, are not able to reliably simulate the adsorption of ions in subnanoporous polarized electrodes (see Figs. 1(a, b)).

Therefore, we modified the CC method guided by experimental and theoretical results showing the key role of chemical defects and subnanopores in the building up of the capacitance(9, 27-34). With this method, there is no additional computational cost compared to classical MD-CC calculations. The local electrostatic field generated by the matrix defects (in the present work non sp²-carbon atoms and edge hydrogen species) drives ion adsorption on the electrode external surface as well as in the whole porosity including the subnanopores. Our electrodes are made of porous carbon texture that is found to be realistic for charcoal, activated carbon as well as for mature kerogen(35, 36). It was obtained using Hybrid reverse Monte Carlo(37) with a density around 1g/cc. Note that our activated carbon texture contains subnanometric pores of 0.5-0.9nm (see Fig. 1(d)). This sharply contrasts from Carbide-Derived-Carbons (CDC) (38) previously used in supercapacitor simulations that only contains pores above 1nm.

We propose a chemically driven charge localization model

(CDCL) that locates partial charges to defective species through the entire electrodes including species at the external or pore surface that are by nature defective. It takes advantage of both CC and CV methods while correcting their main drawbacks opening the path for modelling the adsorption of ions in subnanoporous defective electrodes including the role of doping of elements as such as N, S, F, etc.

We demonstrate that using MD simulations with the COMPASS force field(39, 40) at 300K, the CDCL approach unravels many subnanometric features underlying the physics of ion docking in the charged electrodes ranging from the differentiated desolvation mechanism of cations with respect to anions and their asymmetric adsorption/desorption mechanism inside the nanopores. The pore size distribution shows a maximum at 0.5-0.6 nm (Fig. 1(d)). Sodium and chloride ions can only dock as single bare ions (i.e. unsolvated) in those pores. The electrodes are separated by 30Å on both sides. The system is periodic in all directions and it is initially prepared with 6100 water molecules, 60 sodium and 60 chloride ions in the inter-electrodes regions corresponding to a salt concentration of 0.67 mol/L (see Methods). As shown in Fig. 1(e), the texture of the electrode near the ions contains defects (incomplete rings or rings with 5 members). Fig.1(f) shows the ion density after polarization and we can observe ion docking inside the porous electrodes.

1. Results and discussion

In view of the limitations identified for the CC and the CV method, we have chosen to develop the CDCL approach guided by the chemical attributes of the electrodes. Our electrodes are made of 70% sp² carbon atoms i.e. having three carbon neighbors as immediate neighbors with a typical angle between consecutive carbon atoms around 120 degrees. The other 30% of carbon atoms can be considered as defects where charges are localised (an increase of partial charge for anode atoms, a decrease for cathode species) (41) (see DFT calculations in S.I.).

Upon polarization, DFT calculations show that excess charges in absolute value are localized on the defects or at their vicinity (30). Therefore, the CDCL scheme for the attribution of additional charges consists in applying a Δ_q value to the non-sp² carbon atoms while attributing a null charge to sp² carbon atoms. The sp² character is hereafter determined based on the C-C-C angle between three consecutive carbon atoms (see S.I.). For the sake of simplicity, we assume the following linear formula for the excess charge estimate:

$$\begin{aligned} \Delta_q &= \Delta_{q,max} * (|\Theta - \Theta_{max}|/10) \forall \Theta \in [\Theta_{max} - 10, \Theta_{max} + 10] \\ \Delta_q &= \Delta_{q,max} \forall \Theta \notin [\Theta_{max} - 10, \Theta_{max} + 10] \end{aligned} \quad [1]$$

where Θ_{max} is the value of the C-C-C angle in a perfect sp² matrix (equal to 120 degrees) and $\Delta_{q,max}$ is the maximum excess charge (positive for the anode and negative for the cathode), which magnitude depends on the applied voltage. We calculated that a value of +/- $\Delta_{q,max}=0.0337 e$ gives an excess/deficit average charge on the anode/electrode of Δ_q equals +/- 0.02 e. In order to compare our results with results obtained with the CV method, we have calculated a conversion factor by computing the average charge attributed to the electrode atoms in the CV method. If we apply 1V, the

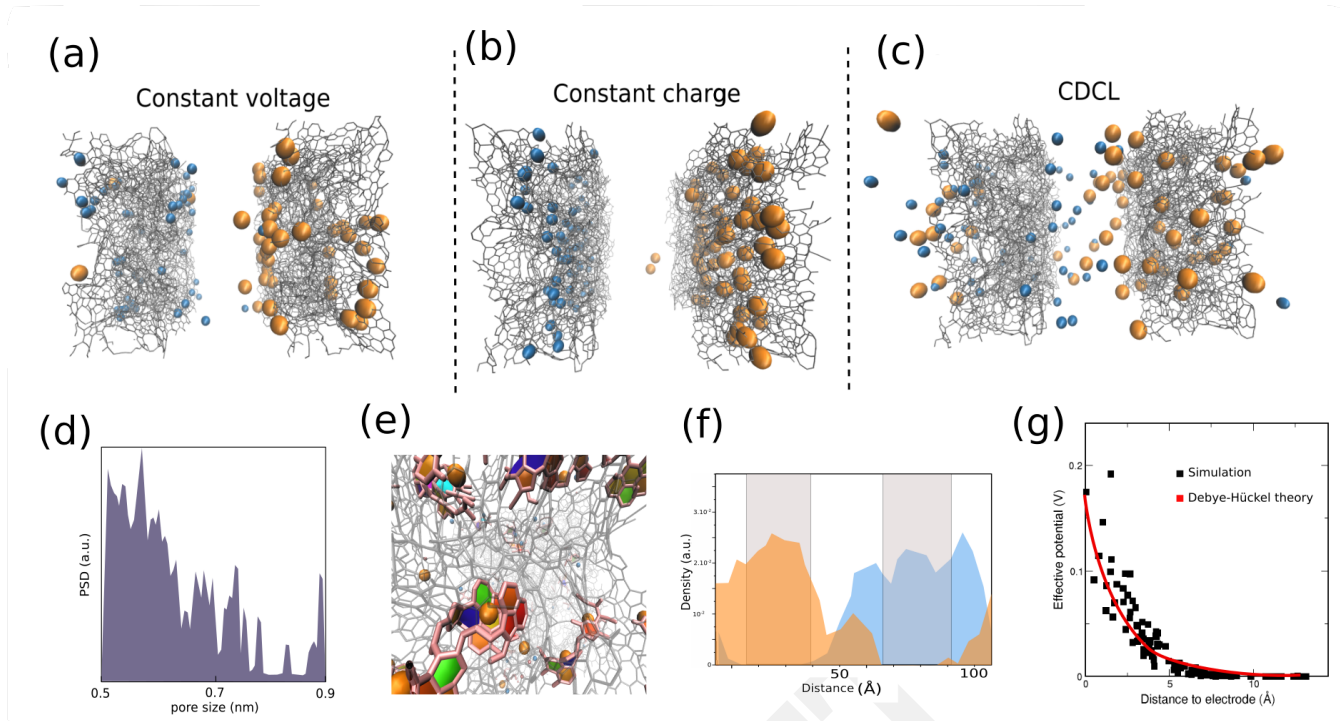


Fig. 1. (a,b and c) Snapshots of the system showing ionic adsorption in different polarisation schemes upon steady state for the constant charge, the constant voltage and the chemistry driven charge localisation schemes respectively. (d) Pore size distribution of the electrodes. (e) structure of the local structure of the porous carbon electrode near adsorption sites. Colored surfaces are guides for the eyes to emphasizing the texture of the pores near the docked-ions. (f) density of Na (in blue) and Cl (in orange) for $\Delta_q = 0.02 e$ (1V) along the simulation cell axis, the two grey bands correspond to the electrodes position and thickness. (g) Calculation of the effective electrical potential acting on the ions in the solution for $\Delta_q = 0.02 e$ (1V). Effective potential acting on the ions in the simulation cell (in black). Due to the roughness, the position of the surface has to be defined arbitrarily, which has been done using the position of the most forward carbon atom of the electrode. Fit obtained using the Debye-Hückel formula (in red). The charge distribution follows a Debye-Hückel law due to the screening of the solution.

170 average excess/deficit charge is $\pm 0.02 e$ per carbon atom on
 171 the anode/cathode respectively, which gives a voltage conversion
 172 factor of 0.02. In the CDCL approach, carbon defective
 173 species have a nominative charge that reflects their local chemical
 174 environment and is in absolute value proportional to the
 175 departure from the perfect sp^2 state (equation 1) and the
 176 applied voltage.

177 Recent CV atomistic simulations of CDCs carbon-based
 178 porous structures have shown that solvated ions are adsorbed
 179 in pores above 1nm in size; no fully dehydrated ions have been
 180 observed implying that the subnanopores are still empty, in
 181 agreement with what we observe in our CV simulations(42).
 182 As demonstrated here below, it is important to note that the
 183 CDCL approach is the only method that is able to predict at
 184 the same time the adsorption of fully dehydrated ions inside
 185 the subnanopores (less than 1 nm, Fig. 1(c)), partially or fully
 186 hydrated ions on the external surface or in any other kind of
 187 larger pores. All confinement environments were experimentally
 188 found to contribute to the overall capacitance of EDL
 189 devices(2).

190 First, we investigate the adsorption of ions on the external
 191 surface of the electrodes. The excess charge imposed additional
 192 Coulombic forces on the ions of the system. The effective
 193 voltage acting on the ions has been computed by extracting
 194 the Coulombic forces on the ions with and without electric field
 195 at the initial time of the simulation. The charge distribution,
 196 in Fig. 1(g), shows that ions close to the external surface of the
 197 electrodes are the ones experiencing larger attraction forces due

213 to the applied voltage compared to ions in bulk electrolyte away
 214 from the electrode surface. Since it is related to a Coulombic
 215 term, the force experienced by the ions is proportional to Δ_q
 216 (see equation 1). The evolution of the effective potential is
 217 characteristic of electrolyte solution and screening effect. Using
 218 the Debye-Hückel formula(43), we can compare the Debye
 219 length obtained from the simulation and that for a solution
 220 with a uniform ion distribution for an ionic concentration of
 221 0.67 mol.L^{-1} (corresponding to the salt concentration in
 222 the inter-electrode void), with a dielectric constant of 80(44).
 223 The agreement between the simulation and the Debye-Hückel
 224 expression for the electric potential at the external surface
 225 of the anode is remarkably good and gives a Debye length
 around 0.2-0.3 nm in quantitative agreement with Debye length
 obtained for this electrolyte type and concentration(44).

213 The number of effective ions adsorbed on and in both porous
 214 electrodes is related to the capacitance of the system. The
 215 capacitance has been calculated and is reported on Fig 2(a) for
 216 each simulation with different Δ_q (the estimation of voltage is
 217 given from the aforementioned conversion). There is a threshold
 218 at low voltage above which ions are being adsorbed on the
 219 external surface of the electrodes (approximately $\Delta_q=0.0025 e$
 220 corresponding to 0.125 V). For larger polarization voltages,
 221 the amount of ions incorporated in the electrodes increases
 222 quasi-linearly until it reached the maximum, hence, the capacitance
 223 exhibits a peak shown in Fig. 2(a) in agreement with the recent
 224 theoretical and simulation work of Verkholyak et al.(45). Note
 225 that at voltages above about 1.8V, we consider

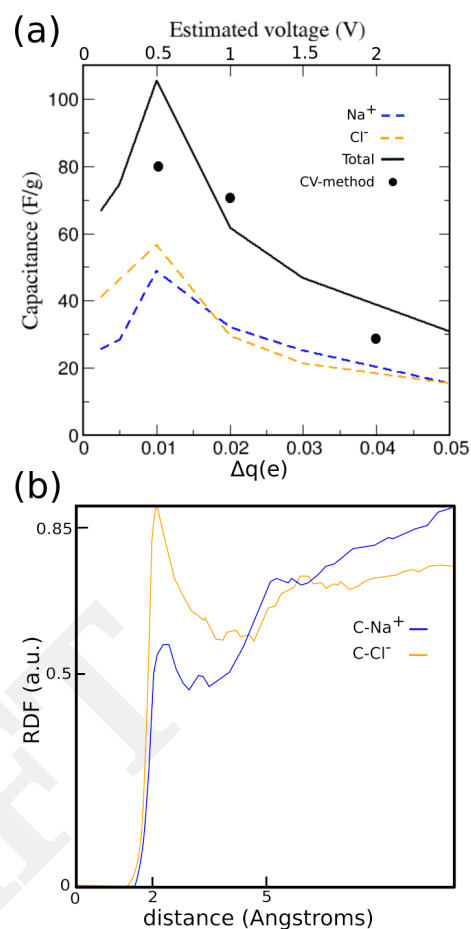
226 that the simulation is probably unrealistic since we do not
 227 consider water splitting that happens at these voltages(46).
 228 The capacitance is in agreement with the typical measured capac-
 229 itance of activated carbons (around 100 F/g with a specific
 230 surface area at around 500 m²/g for our carbon texture) (47).
 231 The maximum capacitance we find, of about 20μF/cm² is in
 232 agreement with experimental values (2, 9, 10). Comparing the
 233 results obtained with the CV and the CDCL on figure 2(a), we
 234 can estimate that the contribution of the subnanopores to the
 235 capacitance is about 20%, meaning that the supercapacitor
 236 made of subnanoporous electrodes remains mostly a standard
 237 EDL device with respect to aqueous electrolytes.

238 Due to the ionic docking in the subnanometric pores, the
 239 capacitance estimated from the CDCL method is larger than
 240 that the one obtained with the CV method (dots, see Fig. 2(a)).
 241 There is a positive correlation between the capacitance and
 242 the specific surface area as measured with BET experiments
 243 (48). In fact the large value of the specific surface area reflects
 244 both the amount of subnanopores and chemical defects on the
 245 carbon backbone. Chloride and sodium contribute differently
 246 to the capacitance (orange and blue dashed lines, see Figs.
 247 2(a)). The adsorption sites are different due to the ionic
 248 size, as shown by the radial distribution function in Fig 2(b).
 249 This leads to an asymmetric loading and charge unbalanced
 250 electrodes, which is a direct consequence of the ion docking
 251 into the subnanometric pores (while the simulation cell overall
 252 charge remains neutral at all times in the simulation). The
 253 capacitance being the sum of the charges divided to the voltage,
 254 the peak can be explained with the less and less efficient ion
 255 docking upon voltage increase, this will be discussed hereafter.

256 In more detail, Figs. 3(a) and (b) show the number of
 257 adsorbed ions on the surface, inside the subnanopores of the
 258 electrodes during polarization simulations and the total ionic
 259 loading during charge and discharge simulations with $\Delta_q =$
 260 0.01e (see S.I. video). At the voltage corresponding to the max-
 261 imum capacitance, the total adsorption is larger for Cl⁻ than
 262 Na⁺. Comparing Figs. 3(a) and (b), one can see that Na⁺
 263 is mostly adsorbed at the external surface whereas Cl⁻ is equally
 264 adsorbed inside and at the external surface of the electrodes.
 265 We observe that half of the sodium ions are adsorbed; the rest
 266 remains in the solution in-between the electrodes. Similarly,
 267 2/3 of the chloride ions are adsorbed and 1/3 remain in the
 268 electrolyte solution.

269 Fig. 3(c) shows the number of adsorbed ions (i) on the sur-
 270 face, (ii) inside the nanopores and (iii) in total for different pol-
 271 arizations. Cl⁻ ions are partially adsorbed on the surface and
 272 inside the electrode nanopores following a monotonous increase
 273 until $\Delta_q=0.01e$ (0.5V) and then it reaches a plateau. Na⁺
 274 is adsorbed in larger quantity than Cl⁻ at voltages larger than
 275 $\Delta_q=0.01e$ (0.5V). Interestingly, as the voltage increases, we
 276 observe a transition from an external surface adsorption only
 277 (from $\Delta_q=0.0025e$ to $\Delta_q=0.01e$) to a dual inside-pore dock-
 278 ing/surface adsorption for the sodium ions above $\Delta_q=0.01e$
 279 (0.5V). This is due to the fact that surface adsorption involves
 280 hydrated ions whereas inside-pore docking involves bare ions.
 281 Low voltages do not provide enough energy to loosen the hydra-
 282 tion shell of Na⁺ leading to external surface adsorption of
 283 hydrated ions (2).

284 The process of ion adsorption in nanopores is accompanied
 285 with a change in the solvation shell of the ions. In bulk water,
 286 sodium ions have a first solvation shell made of approximately 6



287 **Fig. 2.** (a) Capacitance due to sodium and chloride ions adsorbed inside and
 288 onto the electrodes at steady state with a maximum additional charge Δ_q (the
 289 added/subtracted charge is maximal on defective (non-sp²) sites). Note that the
 290 carbon atoms at the vicinity of the pores are not necessarily the non-sp² carbons. The
 291 x-axis represents the excess of charge on each carbon atom of the positive electrode
 292 with respect to Δ_q . The dots correspond to the calculated value with the CV method.
 293 The simulated capacitance value is in the ballpark of experimental values (100 F/g)
 294 for supercapacitors based on porous carbons with specific surface area around 500 m²/g
 295 (which is the value of our simulated porous carbon) (b) Radial distribution functions
 296 for C-Na and C-Cl distances at steady state for $\Delta_q = 0.01e$.

287 water molecules (49), which is also observed in our simulations
 288 before charging the electrodes. An ion and its first layer
 289 hydration shell are of about 0.7 nm in diameter and, therefore,
 290 can only access the largest pores in our system.

291 Fig. 3(d) shows the evolution of the hydration shells of the
 292 adsorbed Na⁺ and Cl⁻ ions together with the total number of
 293 adsorbed ions at $\Delta_q=0.01e$ (0.5V). The adsorbed Na⁺ ions are
 294 surrounded on average by 4-5 water molecules, whereas the
 295 Cl⁻ ions carry 2-3 water molecules. All adsorbed ions have lost
 296 either partially or totally their hydration shell, when adsorbed
 297 on the surface of the electrodes, or their whole hydration shell
 298 when entering the subnanopores. Fig. 3(e) shows the hydration
 299 number of Cl⁻ ions before adsorption and after adsorption
 300 inside the nanopores. The hydration shell becomes loose at
 301 the surface and then the ions can enter either bare or with at
 302 most one water molecule in the subnanopores. Note that we
 303 observed the formation of anion-cation ionic pairs only in the
 304 solution outside of the electrodes.

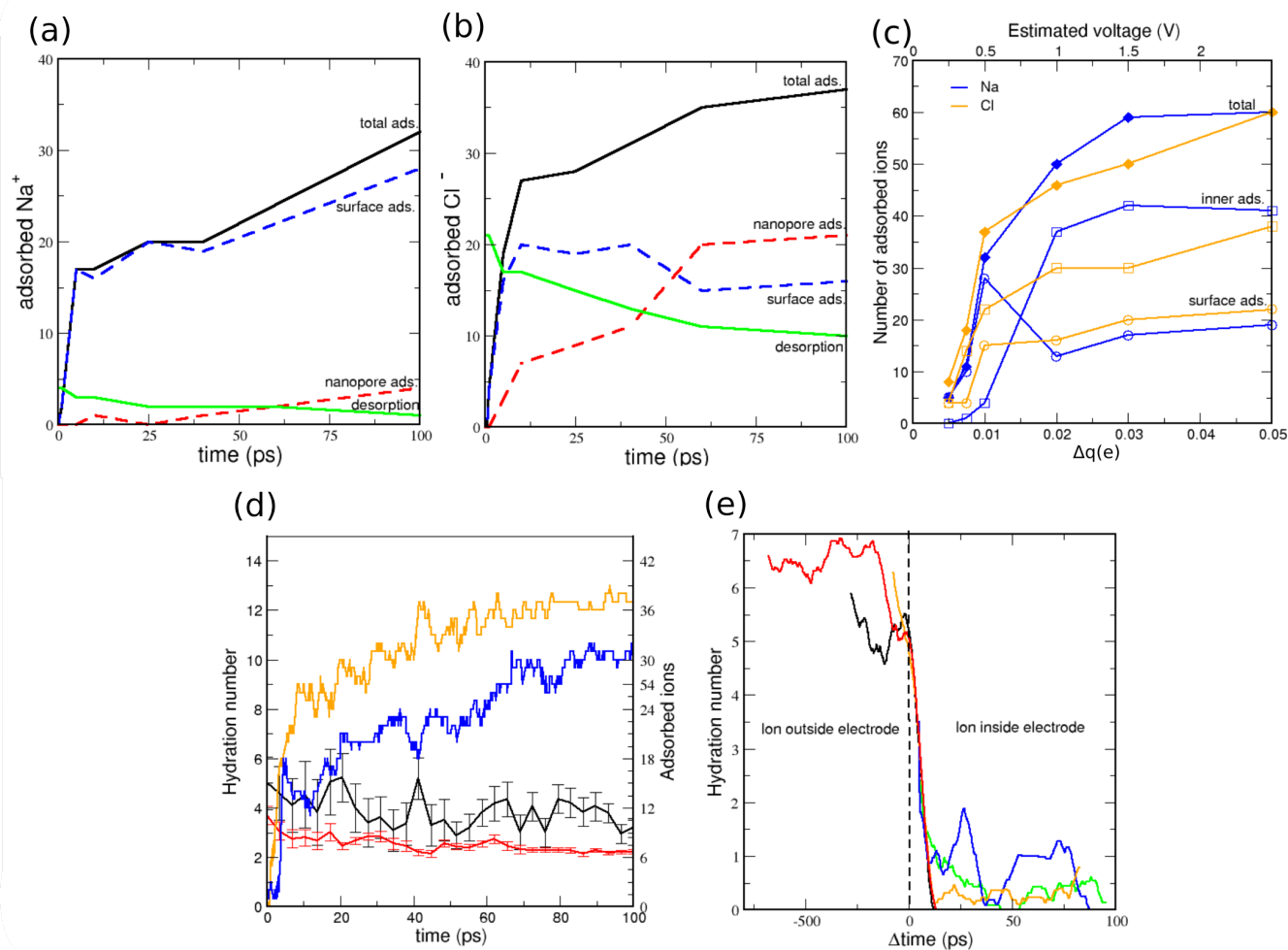


Fig. 3. (a) Evolution of the number of sodium ions in the electrode during the loading, adsorbed in the pore network (blue) or on the surface of the electrode (red) while imposing a voltage corresponding to a $\Delta q = 0.01e$ (0.5V) (total in black) and during unloading (in green) for $\Delta q = 0$. To determine the adsorption, a cutoff of 4.0 Å and 5.0 Å have been used for Na-C and Cl-C distances respectively, corresponding to the first minimum in the radial distribution functions. (b) Evolution of the number of chloride ions in the electrode. (c) Number of (blue) sodium ions and (orange) chloride ions adsorbed (diamond) in total, (squares) inside the electrodes, (circles) at the surface. (d) Evolution of the hydration number during the adsorption around Na (black) and Cl (red) ions and number of ions adsorbed inside the electrodes at $\Delta q = 0.01e$ (0.5V). Error bars correspond to the standard deviation. Evolution of the quantity of adsorbed Na (blue) and Cl (orange). (e) Hydration number of several ions versus Δtime (each color corresponds to a different Na^+ ion), where Δtime is the time difference to the moment where the ion enters into the electrode. The values reported are the running average over 100 steps.

305 Focusing now on the role of water in porous electrodes at
 306 full saturation, we observed that in polarized electrodes that
 307 few water molecules adsorb in the pores of the electrodes (50).
 308 The ratio for the amount of water inside the electrode is less
 309 than 15%. The carbon structure is rather hydrophobic as
 310 indicated by radial distribution functions (shown in S.I.), the
 311 shortest C-water distance being about 3.5 Å .

312 Corrected for the effective accessible pore volume, the sub-
 313 nanopores are just large enough to accommodate one bare ion
 314 (diameter for sodium and chloride equal 0.1nm and 0.18nm
 315 respectively) in agreement with the conclusions of Simon and
 316 Gogotsi(2). While the electrodes are being charged, the den-
 317 sity of water inside the electrodes slightly increases. This
 318 indicates that the adsorption of ions into the carbon electrodes
 319 make the structure less hydrophobic in a similar fashion as
 320 the clay interlayer void is hydrophilic only because the pres-
 321 ence of cations compensating the overall clay layer negative
 322 charge. The clay basal planes per se are rather hydrophobic

323 as they carry no OH surface groups immediately in contact
 324 with adsorbed water; the ions act as water pump inside a
 325 polarized porous carbons or in-between clay layers charged
 326 through isomorphic substitutions (51).

327 In summary, chloride and sodium ions in water are behaving
 328 differently upon working conditions of a supercapacitor (52).
 329 Chloride species appear to be more mobile than sodium ions
 330 that are likely to get trapped in their tighter hydration cage
 331 (53). It also makes chlorides adsorbing faster and at lower
 332 voltage inside the carbon nanopores (see Figs. 3(a) and (b)).

333 Regarding the desorption process, the ions that are ad-
 334 sorbed deep in the core of the electrode will more likely remain
 335 trapped upon discharge. At voltage set back to zero, about
 336 10% of the formerly docked Na^+ ions (about 3% of the total
 337 number of cations) and 30% of the adsorbed Cl^- (about
 338 10% of the total number of anions) are still trapped inside
 339 the electrodes (after 1 ns of unloading, 2 Na^+ and 6 Cl^- are
 340 inside the electrodes, see S.I.). Note that desorption, which is

341 simulated under a null voltage, takes place over a longer time
342 than ion docking (see Figs. 3(a and b)). The trapped ions may
343 not participate to the current unloading cycle but they could
344 move to a nearby pore during the cycling and become again
345 available for storage. The trapped ions upon depolarization
346 is compatible with the hysteretic behavior observed in the
347 supercapacitor I-V characteristic curve. More specifically, the
348 ions that are being desorbed at zero voltage are only the ions
349 that have an easy path to exit the porous material. Other
350 ions, that are in small pores or in tortuous porous network,
351 are not easily extracted from the media. Being smaller ion,
352 Na^+ is often trapped more deeply in the porous network at
353 larger voltages. Three adsorption/desorption cycles has been
354 performed in this work and we have observed that after the
355 first cycle, the amount of ions irreversibly docked inside the
356 electrode nanoporosity remains constant.

357 2. Conclusion

358 We propose a new approach to describe the charge and dis-
359 charge process in subnanoporous carbon made electrodes, in a
360 supercapacitor setting, that we call chemically driven charge
361 localisation model (CDCL). Despite its mean-field charac-
362 ter, the CDCL approach is an improvement of the current
363 standard methods to simulate charged devices at the atomic
364 scale, namely the constant charge and the constant voltage
365 methods that are ineffective to correctly describe ionic dock-
366 ing in subnanopores. Informed from DFT calculations, the
367 CDCL method consists in localising charges on defective non-
368 sp² carbon sites, including chemical or topological defects.
369 By contrast to the standard methods, this allows simulat-
370 ing both adsorption on the electrodes external surfaces and
371 in-subnanopore docking.

372 Applied to a realistic texture of nanoporous carbon, we
373 could unravel the fundamental processes underlying the capac-
374 itive effect of a subnanoporous carbon-based supercapacitor
375 device in operation. We show in particular that subnanomet-
376 ric pores constitute about 20% of the capacitance of such a
377 device using a standard aqueous electrolyte. The simulated
378 value of the capacitance of about 100 F/g (or 20 $\mu\text{F}/\text{cm}^2$)
379 is in good agreement with the experimental values measured
380 on activated carbon based supercapacitors. In more details,
381 we show that the docking of ions in pores is preceded by an
382 assymetrical desolvation at the vicinity of the external pore
383 surface. The ion adsorption density profile on the electrodes
384 external surfaces is in agreement with the Debye-Hückel theory
385 with a Debye length of 0.2-0.3nm. The desolvation process
386 is actually different for sodium and for chloride ions as the
387 hydration shell of sodium is tighter than that of chloride. Once
388 ions are desolvated, they can access nanopores; subnanopores
389 being mostly populated with bare ions in agreement with in
390 situ X-rays experiments (6). Due to the difference in their
391 ionic size, the docking mechanism of sodium and chloride ions,
392 leads to an unbalanced electrode charging. Upon discharge, we
393 found that a significant amount of ions (10% of the cations and
394 30% of the anions) remains trapped in the subnanopores due
395 to the pore network tortuosity right after the first charge that
396 is compatible with the typical I-V curve of supercapacitors.

397 The current CDCL method allows exploring how doping
398 with elements such as N, S, etc. influence the ion adsorption
399 and the in-pore docking(54). Furthermore, the current CDCL
400 method could be coupled with a constant voltage approach in

order to take into account the variation of the substrate defects
charge upon ionic thermal movement. This will allow studying
the ageing of the electrodes texture upon charge-discharge
cycling.

3. Methods

401 A super-capacitor composed by porous carbon layers (of 22Å thick-
402 ness), separated with a water solution containing electrolytes, has
403 been simulated with a fully atomistic approach. The electrodes has
404 been generated using a liquid quench MD method (55) using the
405 reactive force field ReaxFF (56) to obtain a micro-porous carbon
406 containing hydrogen (0.3 H/C). The charges due to defects in the
407 carbon structure are compensated by H atoms. This structure has
408 been relaxed at 293 K and 1 atm, then, cut in half in order to add
409 a phase of bulk of water replacing the other half. The cut leads
410 to unstable atoms at the interface due to broken bonds. Thus, we
411 performed a relaxation with an MD run at a higher temperature
412 (1500 K) to force water molecules to react with the unstable carbon
413 atoms, stabilize the structure and diffuse within the structure. Then,
414 we have duplicated the system one time toward the orthogonal di-
415 rection of the cut surface. Each electrode contains 5440 atoms. It
416 has a connected pore network and a density of 1.45 $\text{g}\cdot\text{cm}^{-3}$.
417

418 In order to study the charge of the capacitor with ions we have
419 built a model in which pure water solution has been enriched with
420 60 Na^+ and 60 Cl^- ions. We have investigated the adsorption of
421 the ions in the porous carbon structure that has been described
422 previously. Since ReaxFF is not well suited for simulating systems
423 with electric fields, the potential used for the charge and discharge
424 simulations is the COMPASS potential (39, 40) to describe the
425 electrodes-water interactions and the SPC/E (57) potential to de-
426 scribe water molecule interactions which is well-known for its good
427 description of polar liquids. The interactions cutoff has been set to
428 12Å. In this work, considering the complexity of the electrodes and
429 therefore of finding a relevant force field to simulate the motion of
430 the atoms of the electrodes, the electrodes were kept rigid. This is
431 an approximation that could slightly influence the quantity of ions
432 that can be adsorbed (in a flexible system, one can imagine that
433 the pores will slightly adapt to the presence of ions). In further
434 studies, the use of reactive force fields such as ReaxFF should be
435 considered in order to assess the stability of the structure and the
436 durability of the pore network due to the ion adsorption. Since
437 such a reactive potential relies on the calculation of charges at each
438 step of the dynamics, the CDCL method should be implemented
439 as a post-calculation to add the charge excess/deficit after the
440 electronegativity equalization method algorithm.

441 Ewald summation has been used for the long range interactions.
442 The PPPM scheme, which is well suited for large systems (in this
443 work over 30 000 atoms), as implemented in LAMMPS has been
444 used with a threshold on the forces of 10^{-4} . Periodic boundary
445 conditions have been imposed to the simulation cell. The electrodes
446 are symmetrical and the simulation cell is electroneutral.

447 For the dynamics, we have used a time step of 0.2 fs, in agree-
448 ment with the frequency of the O-H stretching modes in water.
449 The system has been thermostated using Nosé-Hoover thermostats.
450 Before adding the electric field, the system has been equilibrated
451 during 300ps at 300K. As discussed in S.I., we have not observed
452 any increase of temperature under electric field contrarily to the
453 results published in a recent work by Merlet et al. (26) the authors
454 attribute to a macroscopic dipole moment, which is an artifact of
455 the simulation.

456 **ACKNOWLEDGMENTS.** R.D, P.-L. V and K.I have been sup-
457 ported from the CNRS Momentum grant CEMCAP. Computations
458 have been performed on the GENCI/CINES clusters withing the
459 project A0090911009.

- 460 1. S Chu, A Majumdar, Opportunities and challenges for a sustainable energy future. *Nature* 488, 294–303 (2012).
- 461 2. P Simon, Y Gogotsi, Materials for electrochemical capacitors. *Nat. Mater.* 7, 845–854 (2008).
- 462 3. F Béguin, V Presser, A Balducci, E Frackowiak, Carbons and electrolytes for advanced supercapacitors. *Adv. Mater.* 26, 2219–2251 (2014).
- 463 4. S Porada, R Zhao, A [van der Wal], V Presser, P Biesheuvel, Review on the science and technology of water desalination by capacitive deionization. *Prog. Mater. Sci.* 58, 1388 – 1442 (2013).

- 472 5. ME Suss, et al., Water desalination via capacitive deionization: what is it and what can we
473 expect from it? *Energy Environ. Sci.* **8**, 2296–2319 (2015).
- 474 6. C Prehal, et al., Quantification of ion confinement and desolvation in nanoporous carbon
475 supercapacitors with modelling and in situ x-ray scattering. *Nat. Energy* **2**, 16215 (2017).
- 476 7. S Boukhalifa, et al., In situ small angle neutron scattering revealing ion sorption in microporous
477 carbon electrical double layer capacitors. *ACS Nano* **8**, 2495–2503 (2014) PMID: 24547779.
- 478 8. R Futamura, et al., Partial breaking of the coulombic ordering of ionic liquids confined in
479 carbon nanopores. *Nat. Mater.* **16**, 1225–1232 (2017).
- 480 9. J Chmiola, et al., Anomalous increase in carbon capacitance at pore sizes less than 1
481 nanometer. *Science* **313**, 1760–1763 (2006).
- 482 10. C Merlet, et al., Highly confined ions store charge more efficiently in supercapacitors. *Nat.*
483 *Commun.* **4**, 2701 (2013).
- 484 11. S Kondrat, P Wu, R Qiao, AA Kornyshev, Accelerating charging dynamics in subnanometre
485 pores. *Nat. Mater.* **13**, 387–393 (2014).
- 486 12. H Shao, YC Wu, Z Lin, PL Taberna, P Simon, Nanoporous carbon for electrochemical capac-
487 itive energy storage. *Chem. Soc. Rev.* **49**, 3005–3039 (2020).
- 488 13. M Müller, B Kastening, The double layer of activated carbon electrodes: Part 1. the contribu-
489 tion of ions in the pores. *J. Electroanal. Chem.* **374**, 149–158 (1994).
- 490 14. M Salanne, et al., Efficient storage mechanisms for building better supercapacitors. *Nat.*
491 *Energy* **1**, 16070 (2016).
- 492 15. N Boon, R van Rooij, 'blue energy' from ion adsorption and electrode charging in sea and river
493 water. *Mol. Phys.* **109**, 1229–1241 (2011).
- 494 16. RA Rica, R Ziano, D Salerno, F Mantegazza, D Brogioli, Thermodynamic relation between
495 voltage-concentration dependence and salt adsorption in electrochemical cells. *Phys. Rev.*
496 *Lett.* **109**, 156103 (2012).
- 497 17. P Biesheuvel, R Zhao, S Porada, A [van der Wal], Theory of membrane capacitive deioniza-
498 tion including the effect of the electrode pore space. *J. Colloid Interface Sci.* **360**, 239–248
499 (2011).
- 500 18. JP de Souza, MZ Bazant, Continuum theory of electrostatic correlations at charged surfaces.
501 *The J. Phys. Chem. C* **124**, 11414–11421 (2020).
- 502 19. C Lian, S Zhao, H Liu, J Wu, Time-dependent density functional theory for the charging
503 kinetics of electric double layer containing room-temperature ionic liquids. *The J. Chem.*
504 *Phys.* **145**, 204707 (2016).
- 505 20. L Yang, BH Fishbine, A Migliori, LR Pratt, Molecular simulation of electric double-layer capac-
506 itors based on carbon nanotube forests. *J. Am. Chem. Soc.* **131**, 12373–12376 (2009).
- 507 21. H Liu, CJ Jameson, S Murad, Molecular dynamics simulation of ion selectivity process in
508 nanopores. *Mol. Simul.* **34**, 169–175 (2008).
- 509 22. RK Kalluri, D Konatham, A Striolo, Aqueous nacl solutions within charged carbon-slit pores:
510 Partition coefficients and density distributions from molecular dynamics simulations. *The J.*
511 *Phys. Chem. C* **115**, 13786–13795 (2011).
- 512 23. G Feng, PT Cummings, Supercapacitor capacitance exhibits oscillatory behavior as a func-
513 tion of nanopore size. *The J. Phys. Chem. Lett.* **2**, 2859–2864 (2011).
- 514 24. C Hauf, M Woerner, T Elsaesser, Macroscopic electric polarization and microscopic electron
515 dynamics: Quantitative insight from femtosecond x-ray diffraction. *Phys. Rev. B* **98**, 054306
516 (2018).
- 517 25. T Sun, et al., Rapid electron transfer by the carbon matrix in natural pyrogenic carbon. *Nat.*
518 *Commun.* **8**, 14873 (2017).
- 519 26. C Merlet, et al., Simulating supercapacitors: Can we model electrodes as constant charge
520 surfaces? *The J. Phys. Chem. Lett.* **4**, 264–268 (2013) PMID: 26283432.
- 521 27. SA Evlashin, et al., Role of nitrogen and oxygen in capacitance formation of carbon nanowalls.
522 *The J. Phys. Chem. Lett.* **11**, 4859–4865 (2020) PMID: 32515198.
- 523 28. G Hartmann, GS Hwang, First-principles description of electrocatalytic characteristics of
524 graphene-like materials. *The J. Chem. Phys.* **153**, 214704 (2020).
- 525 29. T Hussain, E Olsson, K Alhameedi, Q Cai, A Karton, Functionalized two-dimensional
526 nanoporous graphene as efficient global anode materials for li-, na-, k-, mg-, and ca-ion
527 batteries. *The J. Phys. Chem. C* **124**, 9734–9745 (2020).
- 528 30. A Maslechko, T Verstraelen, TS van Erp, E Riccardi, Multiscale partial charge estimation on
529 graphene for neutral, doped and charged flakes. *Phys. Chem. Chem. Phys.* **20**, 20678–20687
530 (2018).
- 531 31. D Ibrahim Abouelamaiem, et al., New insights into the electrochemical behaviour of porous
532 carbon electrodes for supercapacitors. *J. Energy Storage* **19**, 337–347 (2018).
- 533 32. ME Suss, et al., Impedance-based study of capacitive porous carbon electrodes with hierar-
534 chical and bimodal porosity. *J. Power Sources* **241**, 266–273 (2013).
- 535 33. F Béguin, V Presser, A Balducci, E Frackowiak, Carbons and electrolytes for advanced super-
536 capacitors. *Adv. Mater.* **26**, 2219–2251 (2014).
- 537 34. J Segalini, B Daffos, P Taberna, Y Gogotsi, P Simon, Qualitative electrochemical impedance
538 spectroscopy study of ion transport into sub-nanometer carbon pores in electrochemical double
539 layer capacitor electrodes. *Electrochimica Acta* **55**, 7489–7494 (2010).
- 540 35. J Pikunic, et al., Structural modeling of porous carbons: Constrained reverse monte carlo
541 method. *Langmuir* **19**, 8565–8582 (2003).
- 542 36. SK Jain, RJM Pellenq, JP Pikunic, KE Gubbins, Molecular modeling of porous carbons using
543 the hybrid reverse monte carlo method. *Langmuir* **22**, 9942–9948 (2006) PMID: 17106983.
- 544 37. C Bousige, A Bojan, FJ Ulm, RJM Pellenq, B Coasne, Optimized molecular reconstruction
545 procedure combining hybrid reverse monte carlo and molecular dynamics. *The J. Chem.*
546 *Phys.* **142**, 114112 (2015).
- 547 38. C Prehal, et al., A carbon nanopore model to quantify structure and kinetics of ion electro-
548 sorption with in situ small-angle x-ray scattering. *Phys. Chem. Chem. Phys.* **19**, 15549–15561
549 (2017).
- 550 39. H Sun, Compass: An ab initio force-field optimized for condensed-phase applications
551 overview with details on alkane and benzene compounds. *The J. Phys. Chem. B* **102**, 7338–
552 7364 (1998).
- 553 40. MJ McQuaid, H Sun, D Rigby, Development and validation of compass force field parameters
554 for molecules with aliphatic azide chains. *J. Comput. Chem.* **25**, 61–71 (2004).
- 555 41. AB Bogeat, Understanding and tuning the electrical conductivity of activated carbon: A state-
of-the-art review. *Critical Rev. Solid State Mater. Sci.* **0**, 1–37 (2019).
42. N Ganfoud, et al., Effect of the carbon microporous structure on the capacitance of aqueous
supercapacitors. *Energy Storage Mater.* **21**, 190–195 (2019).
43. CG Gray, PJ Stiles, Nonlinear electrostatics: the poisson boltzmann equation. *Eur. J. Phys.*
39, 053002 (2018).
44. AM Smith, AA Lee, S Perkin, The electrostatic screening length in concentrated electro-
lytes increases with concentration. *The J. Phys. Chem. Lett.* **7**, 2157–2163 (2016) PMID:
27216986.
45. T Verkholyak, A Kuzmak, S Kondrat, Capacitive energy storage in single-file pores: Exactly
solvable models and simulations. *The J. Chem. Phys.* **155**, 174112 (2021).
46. X Li, et al., Water splitting: From electrode to green energy system. *Nano-Micro Lett.* **12**, 131
(2020).
47. F Barzegar, et al., Investigation of different aqueous electrolytes on the electrochemical per-
formance of activated carbon-based supercapacitors. *RSC Adv.* **5**, 107482–107487 (2015).
48. E Frackowiak, *Electrode Materials with Pseudocapacitive Properties*. (John Wiley and Sons,
Ltd), pp. 207–237 (2013).
49. D Flévit, S Elias, J Hautman, Number of water molecules coupled to the transport of sodium,
potassium and hydrogen ions via gramicidin, nonactin or valinomycin. *Biochim Biophys Acta.*
512, 436–451 (1978).
50. JK Brennan, KT Thomson, KE Gubbins, Adsorption of water in activated carbons: Effects of
pore blocking and connectivity. *Langmuir* **18**, 5438–5447 (2002).
51. D Ebrahimi, RJM Pellenq, AJ Whittle, Nanoscale elastic properties of montmorillonite upon
water adsorption. *Langmuir* **28**, 16855–16863 (2012).
52. G Cassone, F Creazzo, PV Giaquinta, F Saija, A Marco Saitta, Ab initio molecular dynamics
study of an aqueous nacl solution under an electric field. *Phys. Chem. Chem. Phys.* **18**,
23164–23173 (2016).
53. R Mancinelli, A Botti, F Bruni, MA Ricci, AK Soper, Hydration of sodium, potassium, and
chloride ions in solution and the concept of structure maker/breaker. *The J. Phys. Chem. B*
111, 13570–13577 (2007) PMID: 17988114.
54. L Liu, PL Taberna, B Dunn, P Simon, Future directions for electrochemical capacitors. *ACS*
Energy Lett. **0**, 4311–4316 (0).
55. R Ranganathan, S Rokkam, T Desai, P Koblinski, Generation of amorphous carbon models
using liquid quench method: A reactive molecular dynamics study. *Carbon* **113**, 87–99
(2017).
56. ACT van Duin, S Dasgupta, F Lorant, WA Goddard, Reaxff: A Reactive Force Field for Hy-
drocarbons. *The J. Phys. Chem. A* **105**, 9396–9409 (2001).
57. HJC Berendsen, JR Grigera, TP Straatsma, The missing term in effective pair potentials. *The*
J. Phys. Chem. **91**, 6269–6271 (1987).